Available online at www.sciencedirect.com
SCIENCE DIRECT
Catalysis Today 107–108 (2005) 537–544
CATALYSIS TODAY
www.elsevier.com/locate/cattod

# Hydrodesulfurization of dibenzothiophene on $MoS_2$/MCM-41 and $MoS_2$/SBA-15 catalysts prepared by thermal spreading of $MoO_3$

Alvaro Sampieri [a], Stéphane Pronier [b], Juliette Blanchard [a,*], Michèle Breysse [a], Sylvette Brunet [b], Katia Fajerwerg [a], Catherine Louis [a], Guy Pérot [b]

[a] *Laboratoire de Réactivité de Surface, UMR CNRS, Université P. et M. Curie, 4 place Jussieu, 75252 Paris, France*
[b] *Laboratoire de Catalyse en Chimie Organique, UMR 6503 CNRS, Université de Poitiers, 40 avenue du Recteur Pineau, 86022 Poitiers Cedex, France*

Available online 16 August 2005

**Abstract**

$MoS_2$ was dispersed into the porosity of MCM-41 and SBA-15 ordered mesoporous materials by means of thermal spreading of $MoO_3$ oxide, followed by sulfidation. Catalysts with various Mo loadings were prepared (namely 9, 14 and 20 wt%), thoroughly characterized using XRD $N_2$-sorption, and TEM, and their activity in hydrodesulfurization of dibenzothiophene was investigated. Depending on the pore size of the support, a nanocasting of the sulfide particles was observed, and its effect on HDS activity was discussed.


*Keywords:* DBT HDS; Molybdenum sulfide; Mesoporous materials; Nanocasting

## 1. Introduction

Supported CoMoS and NiMoS are widely used in oil refineries for the hydrodesulfurization (HDS) of petroleum-derived feedstocks. Because of new stringent environmental restrictions on the sulfur content of diesel fuel, many attempts have been made to improve their activity [1,2]. One direction of the current research focuses on the use of new types of supports [3–5], and among them on the recently discovered MCM-41 and SBA-15 mesoporous silica materials.

MCM-41 [6,7] and SBA-15 [8,9] are high surface area ordered mesoporous supports with controlled pore size, and these characteristics make them very promising supports for application in oil refining. They are formed by reacting micelles of surfactant with a silica source: their interaction leads to the precipitation of an organised mesophase, and after polymerization of the silica precursor and calcination, an ordered porous structure is obtained. Depending on the choice of the surfactant (cetyltrimethylammonium for MCM-41 or (polyethyleneoxide)$_{20}$(polypropyleneoxide)$_{70}$(polyethyleneoxide)$_{20}$ for SBA-15), and on synthesis conditions, mesoporous materials with honeycomb structure and controlled pore size in the range 2.5–3.5 nm (MCM-41) and 6–9 nm (SBA-15) can be obtained. The rather thin walls of these silica supports (ca. 1 nm for MCM-41 and 3 nm for SBA-15) allow them to develop very high surface areas (ca. 1000 $m^2\ g^{-1}$ for MCM-41 and 800 $m^2\ g^{-1}$ for SBA-15), but are also responsible, especially for MCM-41, for their low stability toward water [10].

The conventional method for the preparation of $MoS_2$ supported catalysts on silica or alumina is the incipient wetness impregnation with an ammonium heptamolybdate solution, followed by calcination and sulfidation [11–14]. However, the moderate stability of mesoporous supports toward water renders alternative methods, such as sonochemical decomposition of molybdenum carbonyl in organic solvent, much more efficient and far less structure-damaging [15,16].

Among those methods, thermal spreading (TS) is of special interest, because it is very simple to achieve. TS is the spontaneous dispersion over macroscopic distances of a metal oxide onto the surface of an oxide support during

* Corresponding author.
*E-mail address:* jblanch@ccr.jussieu.fr (J. Blanchard).

0920-5861/$ – see front matter 
doi:10.1016/j.cattod.2005.07.069

extensive thermal treatment. It leads to the formation of a monolayer or submonolayer of the spread oxide. Thermal spreading of $MoO_3$ is known to occur on many supports, and among them $Al_2O_3$ is the most widely studied. Several possible mechanisms for $MoO_3$ spreading over alumina have been suggested, but recently, Günther et al. have given strong evidence for the gas phase diffusion mechanism, where Mo oxide clusters, probably as $[(MoO_3)_3]$, is evaporated from the $MoO_3$ crystallites and readsorbed on the support surface [17].

Although the mechanism of the thermal spreading of $MoO_3$ on silica surface has been far less studied, and the occurrence of TS on silica has long been controversial, it is now well established that thermal spreading of $MoO_3$ occurs on silica supports, and that the mechanism of the spreading of Mo oxide on silica and alumina are similar. Braun et al. have provided evidence for the formation of dispersed Mo species and small Mo clusters interacting with the silica support using Raman spectroscopy, and of the reaction between surface hydroxyls and $MoO_3$ using FTIR [18,19].

Though thermal spreading of $MoO_3$ is less used than impregnation of ammonium heptamolybdate for the preparation of supported Mo catalyst, it still attracts considerable attention because it leads to the formation of highly dispersed Mo oxide. Furthermore, as long as the impregnation is followed by a calcination step (which is often the case), thermal spreading of Mo oxide will take place during this step, and, as a result, will play a major role on the final dispersion.

TS of $MoO_3$ on MCM-41 has been studied by Li et al. [20,21], who have been able to achieve Mo loading as high as 17 wt% (0.26 g $MoO_3$/g of MCM-41), without major damage to the MCM-41 structure.

In this work, $MoS_2$/SBA-15 and $MoS_2$/MCM-41 catalysts with various Mo loadings are prepared by mechanical mixing followed by thermal spreading. The maximum Mo loading for each type of support is evaluated using XRD and the influence of this treatment on the mesoporous structure is shown using $N_2$-sorption and small angle XRD. Furthermore, an in-depth TEM characterization of the sulfided catalysts is performed to determine how the Mo loading and the pore size of the support influence the stacking and length of the $MoS_2$ slabs and, from this to understand the evolution of the DBT HDS activity with the Mo loading.

## 2. Experimental

### 2.1. Catalysts preparation

MCM-41 and SBA-15 supports are prepared as described elsewhere [8,22–24].

Appropriate amounts of $MoO_3$ (Aldrich, purity 99.99%), and of silica support were finely ground together using a mortar during 30 min to ensure an homogeneous distribution of $MoO_3$. The mechanical mixture was subsequently thermally treated to 773 K (heating rate 1 K $min^{-1}$) during 8 h under He.

A reference $Mo/Al_2O_3$ catalyst was prepared by incipient wetness impregnation of ammonium heptamolybdate (Mo loading 9 wt%) on a commercial $\gamma$-$Al_2O_3$ ($S_{BET}$ = 250 $m^2$ $g^{-1}$), followed by drying at 393 K and calcination under air at 773 K.

Prior to catalytic testing, the samples were sulfided with a 10% $H_2S/H_2$ mixture at 673 K during 14 h under atmospheric pressure to ensure a complete sulfidation of the $MoO_3$ phase.

### 2.2. Characterizations

XRD measurements were carried out using a Siemens D 500 with Cu K$\alpha$ radiation (wavelength $\lambda$ = 1.54 Å).

$N_2$ adsorption–desorption isotherms were obtained on a Micromeritics ASAP 2010 system at 77 K. Before analysis the samples were outgassed at 423 K under a pressure of 0.1 Pa for 5 h. Average pore size was evaluated from the desorption branch of the isotherm using the BJH model.

Transmission electron microscopy measurements of the samples after catalytic test were performed with a Philips CM120 apparatus, with a 0.35 nm resolution equipped with a LaB6 filament. Ultramicrotomy was used to obtain extensive electron-transparent regions, and to ascertain that the observed particles were really located in the porosity of the mesoporous supports. The samples were prepared by embedding the catalyst in a polymer resin, subsequently cured at 343 K for 1 day. Ultramicrotomed slices (circa 50 nm thick) of the embedded sample were cut using a diamond knife, and laid on carbon-covered copper grids. The average lengths and stackings of the $MoS_2$ nanoparticles were estimated from ca. 200 to 300 nanoparticles.

### 2.3. Catalytic activity measurements

Hydrodesulfurization of dibenzothiophene was carried out in a fixed bed reactor under 40 bar total pressure at 513 K. Dibenzothiophene (DBT) was dissolved in decaline

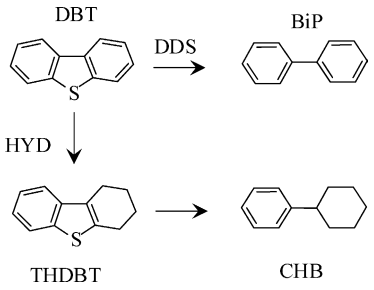


Fig. 1. Scheme of the transformation of dibenzothiophene on hydrotreating catalysts showing the direct desulfurization (DDS) and hydrogenation (HYD) pathways.

(DHN) and the partial pressures of each constituent of the feed were: $P_{H_2} = 30.6$ bar, $P_{DBT} = 0.1$ bar, $P_{DHN} = 9.3$ bar). It has to be noticed that neither $H_2S$ nor $H_2S$ precursor was added to the feed. The products were those shown in Fig. 1 and were the same with all the catalysts. The reaction products were analyzed by on-line gas chromatography using a DB17 (J&W Scientific) capillary column with a temperature program from 373 to 523 K (10 K $min^{-1}$). The activities for the hydrogenation ($a_{HYD} = a_{CHB} + a_{THDBT}$) and direct desulfurization ($a_{DDS}$) pathways were calculated according to Fig. 1, and determined at isoconversion (10–12%).

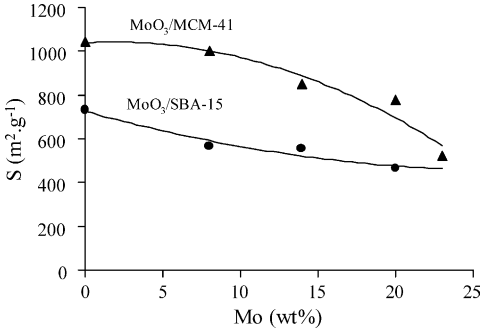


Fig. 3. Evolution of the surface area (BET model) of Mo/MCM-41 and Mo/SBA-15 with the Mo loading (wt%).

## 3. Results

### 3.1. Catalysts characterization

X-ray diffraction is often used in order to check the efficiency of thermal spreading because it allows to detect and quantify undispersed $MoO_3$. The XRD spectra of Mo/MCM-41 and Mo/SBA-15 samples after 8 h thermal spreading are shown in Fig. 2. For samples containing 9 and 14 wt% Mo, the XRD peaks characteristic of the $MoO_3$ orthorhombic phase (JCPDS 76-1003) are either completely absent (MCM-41 support), or very weak (SBA-15 support), indicating that Mo phase was almost fully dispersed. For higher loading however, the peaks of $MoO_3$ can be clearly seen on the diffractogram of the Mo/SBA-15 sample. The amount of undispersed $MoO_3$ has been evaluated from the variation of the intensity of the XRD peak located at $2\theta = 25.7^\circ$ of the mechanical mixture before and after thermal treatment. This amount remains below 1 wt% for all samples except 20% Mo/SBA-15, where it reaches 6 wt%. This means that the amount of actually dispersed Mo is, for this sample, close to 14 wt%, that is almost the same as in 14% Mo/SBA-15 (13 wt%). The lower surface area of SBA-15 compared to MCM-41 (730 compared to 1030 $m^2\ g^{-1}$) might be at the origin of this discrepancy in the maximal amount of fully dispersed Mo. Indeed, the maximal surface loading achieved in this study of fully dispersed Mo is ca. 2 μmol $m^{-2}$ on both SBA-15 and MCM-41 supports (ca. 2.4 μmol $m^{-2}$). This is slightly higher than the value determined by Xie et al. for silica gel (ca. 2 μmol $m^{-2}$) [25] and by Li et al. (1.6 μmol $m^{-2}$) for MCM-41 supports [21], but remains below the limit value experimentally determined by Braun et al. for a non-porous silica (4 μmol $m^{-2}$) [19], indicating that the diffusion of $MoO_3$ might be hindered in porous supports.

As explained in the introductory part, the stability of the mesoporous supports, especially for MCM-41 type supports, is a crucial point. We have therefore checked the evolution of the surface area and mesostructure upon increasing the Mo loading. For both types of supports, the surface area decreases with the Mo loading, but the decrease is stronger on MCM-41 (see Fig. 3). Such evolution of the surface area has been previously reported for MCM-41 by Li et al. [21]. It goes together with a gradual decrease in the pore size, clearly visible for MCM-41 type supports (from 32 Å for the starting material to 26 Å for 20% Mo/MCM-41), but hidden for the SBA-15 supports by the larger pore size and somewhat larger pore size distribution. On the other side, the hexagonal structure of the two supports seems to be preserved even for the higher Mo loading, as can be seen from the low angle X-ray diffractograms of Mo/MCM-41 samples (Fig. 4a) and Mo/SBA-15 (Fig. 4b): whatever the

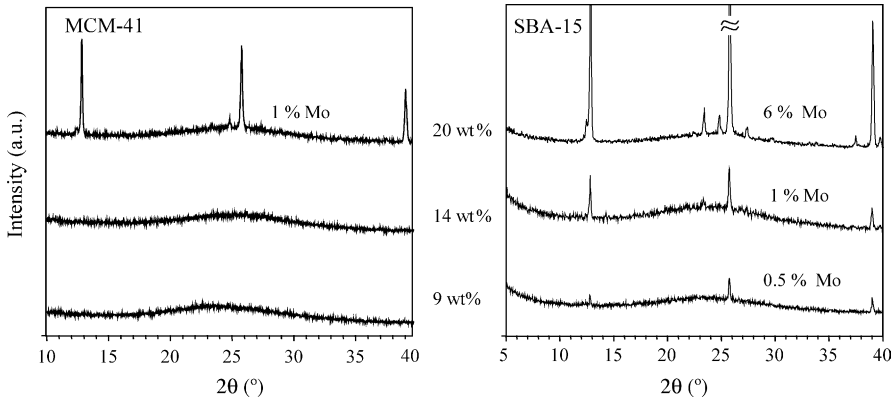


Fig. 2. Wide angle XRD patterns of: Mo/MCM-41 (left) and Mo/SBA-15 (right) with various Mo loading (wt%).

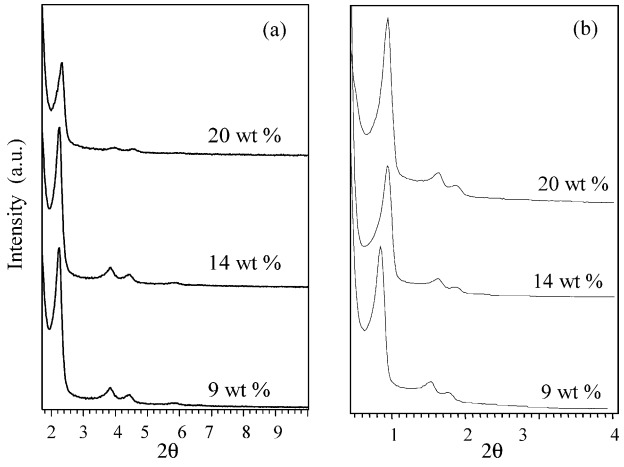


Fig. 4. Small angle X-ray diffraction patterns of (a) Mo/MCM-41 and (b) Mo/SBA-15 with various Mo loadings (wt%).

Mo loading, the three X-ray lines characteristic of the hexagonal structure are clearly visible (the decrease in the intensities of the three X-ray lines with the Mo loading observed for the MCM-41 supported samples might be partially due to the fact that Mo is a strong X-ray absorber). The strong decrease in surface area observed for the Mo/MCM-41 samples would therefore be partially due to pore blocking by the $MoO_3$ phase.

Fig. 5 shows a low magnification picture of sulfided 14% Mo/MCM-41 together with two enlargements. The top view (with moderate enlargement) provides evidences for the conservation of the mesostructure after catalytic test, and for the homogeneous dispersion of $MoS_2$ throughout the MCM-41 grain. Furthermore, it shows two kinds of view of the mesostructure: a front view on the top left corner (left frame), with the honeycomb structure, and on most of the rest of the picture a side view of the bent channels. On both views, it is possible to distinguish the presence of $MoS_2$, either as dark black spots on the front view or as grey rods, whose orientation appears to match the one of the tubular channels (side view).

The two bottom pictures, which have been taken with a higher magnification, allow a better observation of these two types of view. On these two pictures, the structure of the mesoporous support is not seen anymore, due to its collapse at high beam energy. However, it is possible to distinguish the $MoS_2$ slabs, and to determine their length and stacking. The two views appear to be quite different regarding the $MoS_2$ nanoparticles. First, the front view (bottom left) shows small randomly oriented $MoS_2$ nanoparticles having all a

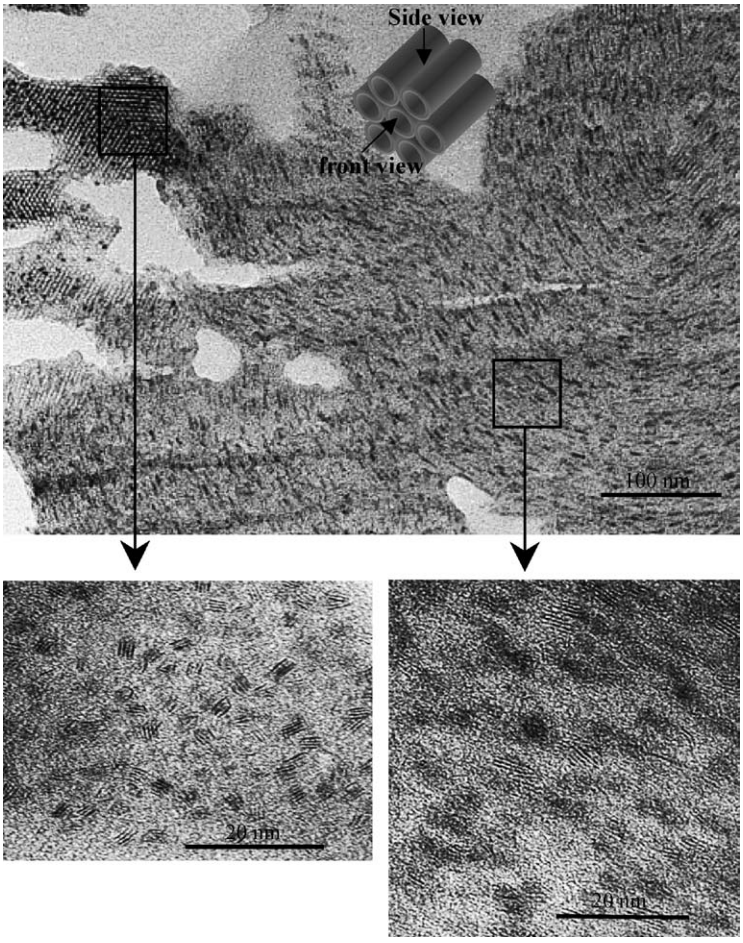


Fig. 5. TEM micrographs of sulfided 14% Mo/MCM-41 (top: general view; bottom left: front view; bottom right: side view) after catalytic test.

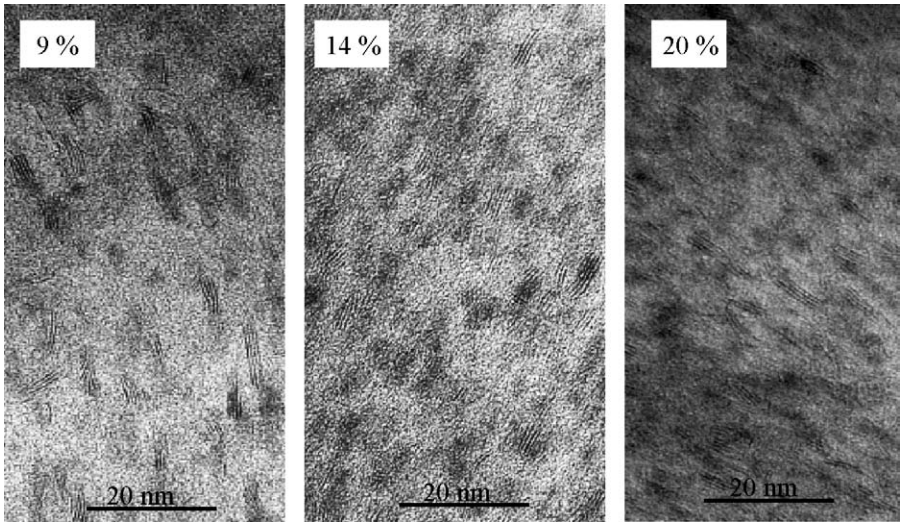


Fig. 6. TEM micrographs of sulfided 9% Mo/MCM-41(left), 14% Mo/MCM-41 (middle) and 20% Mo/MCM-41 (right) after catalytic test.

slab length of ca. 2.5 nm, and with, most of the time, a stacking of 3 or 4 (average stacking 3.5). Second, the side view (bottom right) shows elongated slabs (average stacking of 3.3, average length of 3.5), which appears to display a common orientation. Together with these slabs, grey rods having the same orientation and length, can be detected. The observation of ''spots'' (in addition to the usual $MoS_2$ slabs) has been reported after mild sulfidation of Mo and NiW supported catalysts. They were assigned to nanometer size spherical entities of Mo (respectively, NiW) sulfide and/or oxysulfide [26,27]. However, their observation by TEM necessitates quasi in situ sulfidation, due to their high sensitivity to exposure to air. Therefore, the grey rods we observe are unlikely to be due to these entities, and are more probably due to stackings of $MoS_2$ slabs, whose orientation with regards to the electron beam is highly tilted, as already proposed by Zaikovskii et al. [28].

The three TEM pictures displayed in Fig. 6, correspond to sulfided Mo/MCM-41 with three different Mo loadings (9, 14 and 20%). In all cases elongated $MoS_2$ nanoparticles can be observed, either as a stacking of slabs or as grey rods. The average size and stacking do not appear to be modified by an increase in the Mo loading, and the only change is an increase in the density of particles.

Fig. 7 shows two TEM pictures of sulfided 14% Mo/SBA-15: on the left a front view, on the right a side view. The mesostructure is still clearly visible (honeycomb structure on the left picture and parallel channels on the right), indicating that the stability of SBA-15 to high energy beam, is better than that of MCM-41 support, probably due to its thicker walls. On all the pictures, and whatever the loading (9 or 14%), $MoS_2$ slabs are hardly seen on this support, and are mostly present as isolated slabs or bunch of two, or three slabs. These slabs seem either to be partially embedded in the silica walls, or, more probably, to stick to walls, leaving the porosity almost completely free. The average size and stacking, as calculated from the front and the side view are very close (average size 2.8 nm, average stacking 2, but the actual stacking might be somewhat lower, because isolated slabs are difficult to detect reliably). No specific orientation of the slabs along the channel can be observed.

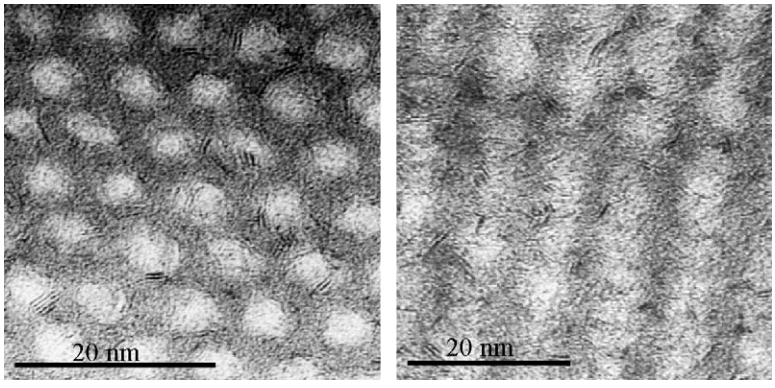


Fig. 7. TEM micrographs of sulfided 14Mo%/SBA-15 (left: front view; right: side view) after catalytic test.

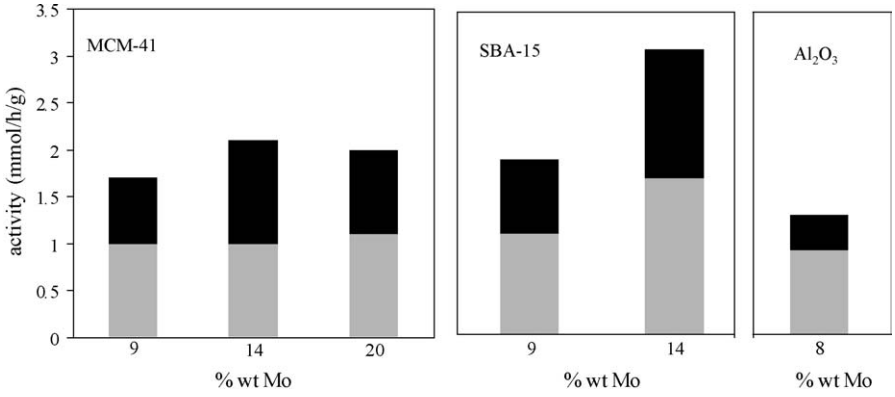


Fig. 8. $a_{HYD}$ (black) and $a_{DDS}$ (grey) of Mo/MCM-41 (left), Mo/SBA-15 (middle) and reference $Mo/Al_2O_3$ (513 K, 40 and 0.1 bar DBT).

### 3.2. Hydrodesulfurization of dibenzothiophene

The HYD and DDS activities for MCM-41 and SBA-15 supported catalysts, and for the reference $Mo/Al_2O_3$ are shown on Fig. 8. The activities and $a_{HYD}/a_{DDS}$ ratios of the 9% Mo/MCM-41 and 9% Mo/SBA-15 are close and higher than those of the reference 8% $Mo/Al_2O_3$. The $a_{HYD}/a_{DDS}$ ratio of the two Mo/silica supports is not significantly modified upon increasing the Mo loading, but the variation of the activity with the loading differs for MCM-41 and SBA-15. For MCM-41 supported catalysts, the overall activity hardly increases upon increasing the loading to 14%, and decreases upon increasing further the loading to 20%. On the other hand, the overall activity is multiplied by 1.6 between 9 and 14% Mo loading for SBA-15 supported catalysts. This value is actually very close to the ratio of the loadings (1.55), so that, between 9 and 14%, the increase in the activity appears to linearly depend on the Mo loading. The origin of the discrepancy between the two supports will be discussed in the last part.

## 4. Discussion

Hensen et al. [29] have shown that the weak interactions between silica and molybdenum result in a low and inhomogeneous dispersion of the $MoS_2$ phase, but also in a higher stacking of the $MoS_2$ slabs than on alumina support. According to the authors, this higher stacking is responsible for the observed higher DBT HDS intrinsic activity of $Mo/SiO_2$ compared to $Mo/Al_2O_3$. Our TEM results indicate that a high and homogeneous dispersion of $MoS_2$ on silica can be achieved, provided that high surface area silica supports, and appropriate synthesis conditions are used. Furthermore the positive effect of silica supports on the overall HDS activity of the $MoS_2$ phase is confirmed, but surprisingly it is accompanied by a major modification of the $a_{HYD}/a_{DDS}$ ratio equal to 0.38 for the alumina supported catalyst, it varies between 0.75 and 1.05 for the silica supported catalysts. It is closer to the value determined for silica–alumina support by Hensen et al. using similar experimental conditions ($P_{H_2S} = 0$): $a_{HYD}/a_{DDS}$ was equal to 0.17 for $Mo/Al_2O_3$, to 0.21 for $Mo/SiO_2$, and to 0.62 for Mo/silica–alumina [29]. Moreover, although the stacking of $MoS_2$ on SBA-15 support is lower than on MCM-41 support, the selectivities are close. The $a_{HYD}/a_{DDS}$ ratio varies between 0.75 and 1.05 for the MCM-41 support, and between 0.75 and 0.85 on the SBA-15 support. The relationship between the stacking of the $MoS_2$ slabs and the DBT HDS activity and selectivity remains therefore less straightforward than proposed by Hensen et al., and the higher activities of 9% Mo/SBA-15 and 9% Mo/MCM-41 compared to 8.0% $Mo/Al_2O_3$ is probably mainly connected to the high dispersion of the $MoS_2$ phase on the mesoporous supports.

Another important result of this study is that the effect of the Mo loading on the overall DBT HDS activity seems to depend on the choice of the silica support. Indeed, from the high, and loading-independent dispersion of $MoS_2$ in both types of supports, one would expect a linear increase in the HDS activity upon increasing the loading. This is actually true only for SBA-15 supported catalysts, and not for MCM-41 supported catalysts, for which the activity is hardly modified between 9 and 20 wt% Mo loading (Fig. 8). The reason for this is probably due to the major differences in the structure of these two series of catalysts as revealed by TEM. The TEM pictures of the SBA-15 clearly show that the $MoS_2$ particles stick to the silica walls and that the porosity is free, which should favour the access of the reactant to the catalytic site. On the opposite, for the Mo/MCM-41 catalysts, the access to the catalytic sites is much more doubtful. Indeed the striking differences between the front and the side views of the mesostructure (Fig. 5), together with the average values of slabs length and stacking determined from the TEM pictures, led us to consider a nanocasting of the $MoS_2$ nanoparticles by the MCM-41 tubular porosity:

- The average length, as determined from the front view, is ca. 2.5 nm, and a stacking of 3–4 corresponds to a width of 2.0–2.6 nm (considering the $d$-spacing of $MoS_2$ phase $d_{0\,0\,2} = 6.1$ Å), so that the $MoS_2$ particles detected on the front view appear to have a circular shape, with a diameter

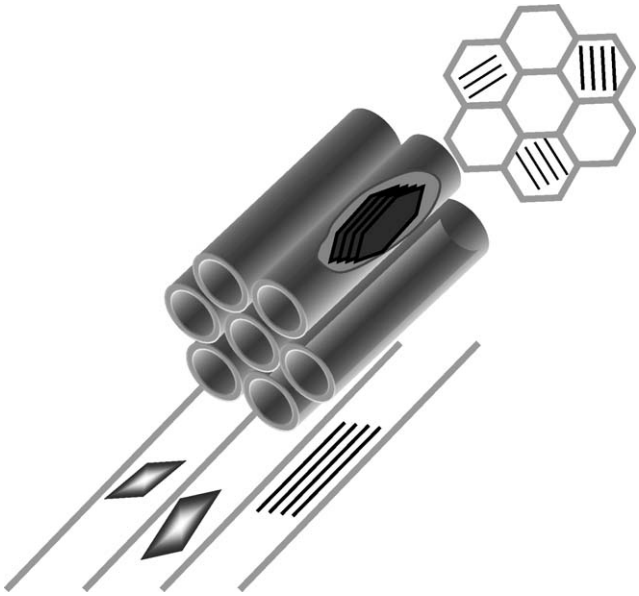

Fig. 9. 3D view and the two corresponding projections showing $MoS_2$ slabs casted into the pores of a MCM-41 mesoporous material.

close to the one of the inner diameter of the support (ca. 3 nm).

- The average length on the side view is ca. 3.5 nm, and the stacking is the same as on the front view. Furthermore, almost all the slabs have a common orientation, parallel to the support channels (Fig. 5).

The front and side views together with the 3D drawing reconstructed from these two views are shown on Fig. 9. On the side view, the nanoparticles appear either as a stacking of slabs or as blurred elongated patches depending on their orientation with respect to the beam.

This casting of the $MoS_2$ particles by the MCM-41 pores could of course lead to serious limitations in the access to the active sites, and one can expect these limitations to grow with the Mo loading. The increase of the Mo loading will indeed lead to an increasing number of $MoS_2$ particles per MCM-41 channel, and therefore to an increasing number of $MoS_2$ particles whose access is prevented. A rough estimation of the distance between two $MoS_2$ particles in a channel, give a value of 0.2 μm for a Mo weight loading of 9% and of 0.09 μm for a loading of 20%. It is not easy to evaluate the length of the MCM-41 channels from the TEM pictures because, as can be seen on Fig. 5, (i) the MCM-41 grains have an inner macroporosity and (ii) the tubular channels are bent. For example, for an average length of 0.5 μm, the access to 20% of the particles will be hindered for a Mo loading of 9%, and to 60% for a loading of 20%.

## 5. Conclusion

In this work, $MoS_2$/SBA-15 and $MoS_2$/MCM-41 catalysts with Mo loadings as high as 20% were prepared without serious damage to the support structure. The maximum amount of fully dispersed Mo (14% for Mo/SBA-15 and 20% for Mo/MCM-41) was close to the value previously determined for this kind of supports and seemed to depend mainly on the surface area of the starting support. Whatever the Mo loading and the support, a high dispersion of the active phase was observed using TEM. For SBA-15 supported catalysts the $MoS_2$ slabs appeared to be oriented at random in the porosity of the support and an average $MoS_2$ slabs length of 2.8 nm and a stacking of 2 was determined. For MCM-41 supported catalysts, anisotropic $MoS_2$ particles lined up with the mesoporous channels were observed, whose stacking and length matched the pore size of the support. This finding is a very explicit example of how the tubular channel of the MCM-41 support can influence the growth of a crystalline phase in their porosity. The fact that the DBT HDS activity for the MCM-41 supported catalysts did not increase with the Mo loading was assigned to this nanocasting of the $MoS_2$ particles, which prevents the access of the reactant to the active sites.

## Acknowledgements

This work has been supported by a Ph.D. grant from CONACYT (Mexico) and SFERE (France).

## References

[1] S.K. Bej, S.K. Maity, U.T. Turaga, Energy Fuels 18 (2004) 1227–1237.
[2] M. Breysse, G. Djega-Mariadassou, S. Pessayre, C. Geantet, M. Vrinat, G. Perot, M. Lemaire, Catal. Today 84 (2003) 129–138.
[3] G. Perot, Catal. Today 86 (2003) 111–128.
[4] J. Cejka, Appl. Catal. A 254 (2003) 327–338.
[5] Y. Saih, K. Segawa, Catal. Today 86 (2003) 61–72.
[6] J.S. Beck, J.C. Vartuli, W.J. Roth, M.E. Leonowicz, C.T. Kresge, K.D. Schmitt, C.T.-W. Chu, D.H. Olson, E.W. Sheppard, S.B. McCullen, J.B. Higgins, J.L. Schlenker, J. Am. Chem. Soc. 114 (1992) 10834–10843.
[7] C.T. Kresge, M.E. Leonowicz, W.J. Roth, J.C. Vartuli, J.S. Beck, Nature 359 (1992) 710–712.
[8] D. Zhao, Q. Huo, J. Feng, B.F. Chmelka, G.D. Stucky, J. Am. Chem. Soc. 120 (1998) 6024–6036.
[9] D. Zhao, J. Feng, H. Qisheng, N. Melosh, G.H. Fredrickson, B.F. Chmelka, G.D. Stucky, Science 279 (1998) 548–552.
[10] M. Carrott, A.J.E. Candeias, P.J.M. Carrott, K.K. Unger, Langmuir 15 (1999) 8895–8901.
[11] M. Breysse, J.L. Portefaix, M. Vrinat, Catal. Today 10 (1991) 489–505.
[12] I.E. Wachs, Chem. Eng. Sci. 45 (1990) 2561–2565.
[13] C. Song, K.M. Reddy, Appl. Catal. A 176 (1999) 1–10.
[14] K.M. Reddy, B. Wei, C. Song, Catal. Today 43 (1998) 261–272.
[15] M.V. Landau, L. Vradman, M. Herskowitz, Y. Koltypin, A. Gedanken, J. Catal. 201 (2001) 22–36.
[16] A. Gedanken, X.H. Tang, Y.Q. Wang, N. Perkas, Y. Koltypin, M.V. Landau, L. Vradman, M. Herskowitz, Chem. Eur. J. 7 (2001) 4546–4552.
[17] S. Günther, F. Esch, L. Gregoratti, A. Barinov, M. Kiskinova, E. Taglauer, H. Knözinger, J. Phys. Chem. (2004) ACS ASAP.
[18] S. Braun, L.G. Appel, M. Schmal, Appl. Surf. Sci. 201 (2002) 227–235.

[19] S. Braun, L.G. Appel, V.L. Camorim, M. Schmal, J. Phys. Chem. B 104 (2000) 6584–6590.
[20] Z. Li, L. Gao, S. Zheng, Mater. Lett. 57 (2003) 4605–4610.
[21] Z. Li, L. Gao, S. Zheng, Appl. Catal. A 236 (2002) 163–171.
[22] A. Martins, J.M. Silva, J. Blanchard, P. Massiani, M. Breysse, F.R. Ribeiro, M.F. Ribeiro, React. Kinet. Catal. Lett. 82 (2004) 139–147.
[23] P. Tian, J. Blanchard, K. Fajerwerg, M. Breysse, M. Vrinat, Z.M. Liu, Microporous Mesoporous Mater. 60 (2003) 197–206.
[24] J.M. Kim, S. Jun, R. Ryoo, J. Phys. Chem. B 103 (1999) 6200–6205.
[25] Y. Xie, Y. Tang, in: D.D. Eley, H. Pines, P.B. Weisz (Eds.), Advance Catalysis, vol. 37, Academic Press, London, 1990, pp. 1–43.
[26] H.R. Reinhoudt, A.D. Van Langeveld, P.J. Kooyman, R.M. Stockmann, R. Prins, H.W. Zandbergen, J.A. Moulijn, J. Catal. 179 (1998) 443–450.
[27] P.J. Kooyman, E.J.M. Hensen, A.M. De Jong, J.W. Niemantsverdriet, J.A.R. Van Veen, Catal. Lett. 74 (2001) 49–53.
[28] V.I. Zaikovskii, L.M. Plyasova, V.A. Burmistrov, A.N. Startsev, Y.I. Ermakov, Appl. Catal. 11 (1984) 15–27.
[29] E.J.M. Hensen, P.J. Kooyman, Y. van der Meer, A.M. van der Kraan, V.H.J. de Beer, J.A.R. van Veen, R.A. van Santen, J. Catal. 199 (2001) 224–235.